Vibrational Spectroscopy Methods as a Powerful Tool for Nanomaterials Characterization

M. Šćepanović, Z. Dohčević-Mitrović, M. Grujić-Brojčin, and Z. V. Popović

Center for Solid State Physics and New Materials, Institute of Physics, Pregrevica 118, 11080 Belgrade, Serbia

Abstract. The use of the Raman and infrared spectroscopy techniques in characterization of nanostructured materials is presented. The structural characterization, estimation of average grain size and size distribution, layer thickness, strain effects, presence of defects, phase separation and nonstoichiometry by Raman spectroscopy is illustrated in the case of CeO_2, doped CeO_2, anatase TiO_2, and ZnO nanopowders, as well as nanostructured $ZnSe/SiO_x$ multilayers. Temperature dependence of Raman spectra of CeO_2, doped CeO_2 and TiO_2 nanopowders has been specially analyzed. The shift and broadening of the Raman modes in these nanopowders are dominated by the strong confinement, inhomogeneous strain and nonstoichiometry at lower temperatures. However, change in their Raman spectra by heating indicates the predominance of anharmonic processes up to 500^{o}C, while at higher temperatures their behavior resembles more to the bulk. On the other side, the shift and broadening of Raman modes in ZnO powders are ascribed to the tensile strain increasing with activation time. Adequacy of one-dimensional (1D) confinement model for analyzing of the shift and asymmetric broadening of Raman mode in nanostructured $ZnSe/SiO_x$ multilayers is also demonstrated. Infrared spectroscopy method has been applied on TiO_2 and ZnO nanopowders in analysis of grain size and shape, porosity and nonstoichiometric defects.

INTRODUCTION

Raman spectroscopy is powerful tool for characterization of nano-sized materials and structures. It is widely used for a study of phonon confinement effects, the effect of the increase of local temperature, strain and substitutional effects, lattice distortion, presence of structure defects and nonstoichiometry in different kinds of nanomaterials. Recent progress in use of the Raman spectroscopy for nanomaterials characterization is summarized in Ref. [1].

Several factors like phonon confinement [2-8], strain [6, 9], non–homogeneity of the size distribution [6, 10], defects and nonstoichiometry [6, 11], as well as anharmonic effects due to temperature increase [12] can contribute to the changes in the peak position, linewidth and shape of the Raman modes in nanostructures. The factors which play an important role in Raman spectra depend on the structural characteristics of nanomaterials, first of all the dimensionality of nanostructure [8, 13]. The grain size and its distribution, existence of mixed phases, value and type of the strain (compressive or tensile), discrepancy from stoichiometry as well as the type of

stoichiometric defects, etc. have great influence on Raman spectra of nanomaterials. We shall demonstrate here how Raman spectroscopy method can be used for characterization of nano-powdered oxides like TiO_2, CeO_2 and ZnO, as well as nanostructured $ZnSe/SiO_x$ multilayers.

The shift, broadening and asymmetric shape of Raman modes, observed in these nanomaterials, are compared to spectra obtained from the phenomenological model, which takes into account disorder effects through the breakdown of the k=0 Raman-scattering selection rule, as well as the anharmonicity, which is incorporated through the 3- and 4-phonon decay processes. The application of three-dimensional (3D) confinement model, appropriate for isolated or loosely connected nanoparticles, shows that the shift and broadening of the Raman peak in some nanopowders are dominated by the strong confinement and inhomogeneous strain (CeO_2) [14], while in the others anharmonic effects (TiO_2) [15] or tensile strain (ZnO) [16] plays the main role. On the other side, the shift and asymmetric broadening of Raman mode in nanostructured $ZnSe/SiO_x$ multilayers is analyzed by one-dimensional (1D) confinement model, appropriate for very thin films or quantum wells [17]. Due to low dimensions of these structures the surface phonon modes are also observed [17].

CeO_2, doped CeO_2 [18] and anatase TiO_2 [19] nanopowders were temperature treated in order to investigate the phonon behavior and stability of these nanocrystalline materials. Temperature dependence of Raman spectra of these nanomaterials has specially analyzed.

Infrared (IR) spectra of nanocrystalline solids defer from spectra of monocrystal due to polycrystalline character and island structure of nanoparticles. From IR spectra it is possible to get information about the energy gap, grain size, porosity, nature of the surface bonds, and chemical reactions occurring at the nanoparticle surface.

Applying the effective medium theories (EMA) to interpret the IR reflectivity spectra of TiO_2 nanopowders we established the relation between the spectra shape and porosity of nanopowders [20]. Model for IR spectra based on generalized Bruggeman EMA, including factorized form of dielectric function is used to analyze the plasmon contribution which originate from nonstoichiometric defects in TiO_2 nanopowder [21].

Differences between IR reflection spectra of mechanically activated and commercial ZnO powders pointed out to the changes in the powder microstructure, as well as the presence of unintentionally introduced impurities during the activation [22].

RESULTS OF RAMAN SPECTROSCOPY

Raman spectra of CeO_2 and doped CeO_2 nanopowders

Fig. 1(a) shows Raman spectra of $CeO_{2-\delta}$ and $Ce(Nd,Gd,Ba)O_{2-\delta}$ samples at room temperature before and after heat treatment [18]. It is interesting to note that Raman modes of only CeO_2 and $Ce(Ba)O_2$ samples becomes symmetric after annealing, almost at the same position as in bulk sample. The Raman mode in Nd-doped sample stays asymmetric, although the mode frequency shifts to higher energies while

linewidth becomes smaller. The most interesting is the case of $Ce_{0.85}Gd_{0.15}O_2$. After annealing the Raman mode becomes narrow but asymmetric. By deconvolution using Lorentz-line profile technique we have found that this mode consists of two modes with frequencies of 464 and 487 cm^{-1}. As XRD diffraction peaks of CeO_2 and Gd_2O_3 coincide in many cases, the XRD analysis seams to be inadequate technique for investigation of the CeO_2-Gd_2O_3 system. Contrary to that, Raman spectra of these samples show clear evidence of phase separation even in the lowest Gd_2O_3 concentration (20%) case, Fig. 1b. Namely, the Raman peak of CeO_2, which appears at about 464 cm^{-1} in polycrystalline sample, can be observed in the 20% Gd_2O_3 sample at the same frequency. Besides this line, one additional mode can be easy resolved at about 487 cm^{-1}, which belongs to Gd_2O_3. An increase of Gd_2O_3 concentration leads to an intensity decrease (increase) of CeO_2 (Gd_2O_3) Raman mode.

This study has shown that in Raman spectra of as-grown CeO_2 and doped CeO_2 strong phonon confinement and inhomogeneous strain play main role, while the anharmonic processes and crystallite growth become predominant by heating.

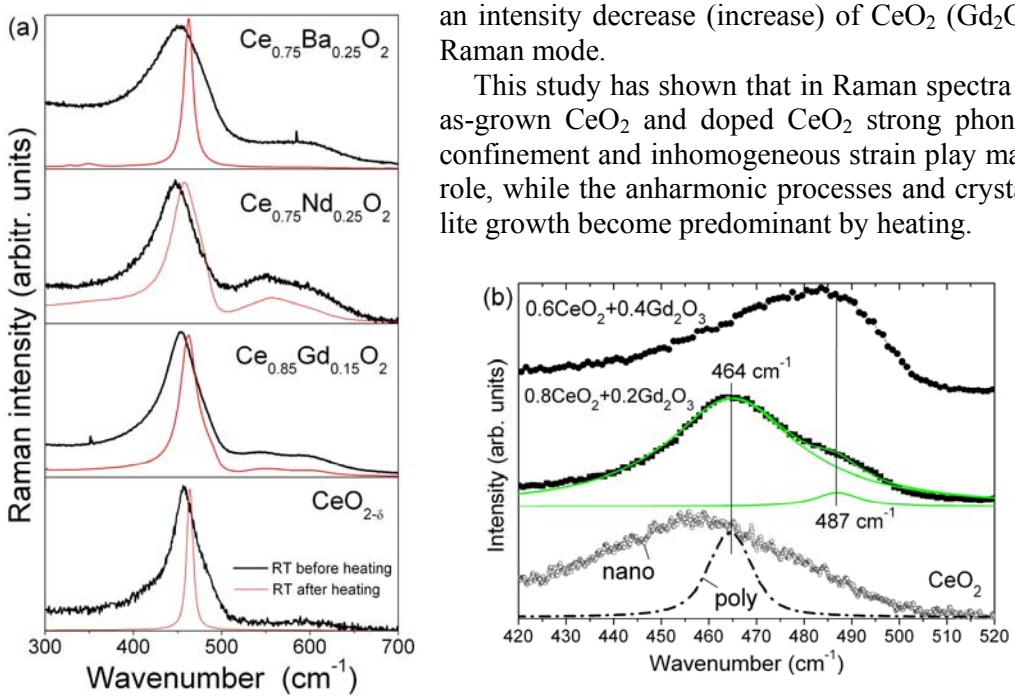

FIGURE 1. Raman spectra of cerium oxide doped samples at room temperature (RT) before and after annealing to 1000°C (a). Room temperature Raman spectra of CeO_2 polycrystalline and nano-sized samples together with Raman spectra of 20 % and 40% CeO_2-Gd_2O_3 samples (b).

Raman spectra of anatase TiO_2 nanopowder

Commercial TiO_2 nanopowder in anatase phase was temperature treated in order to investigate the phonon behavior and stability of this nanocrystalline material [19]. The Raman spectra of anatase TiO_2 nanocrystals measured in the temperature range 23-1173 K are shown in Fig. 2(a). The variations of the frequency and linewidth of Raman modes with temperature are evident. The blueshift and broadening of the lowest frequency E_g Raman mode are particularly analyzed by the phonon confinement model, including anisotropic dispersion relations with temperature

dependant parameters. It is evident that frequency and linewidth increase by heating above room temperature, while the lineshape of E_g mode becomes more symmetric. As-read experimental (open symbols) and calculated (full symbols) positions and halfwidths of Raman E_g mode are compared in Fig. 2(b). The influence of phonon confinement effect can be estimated through the difference between measured and calculated values, which decreases with temperature increase above 773 K (500°C). It is related to the crystallite size increase shown in Fig. 2(c), obtained by fitting procedure. This coincides with the results of Balaji et al. [23], where upon annealing at temperature at and below 400°C the cristallite size do not change significantly, while this size grows continuously as the annealing temperature is raised to 900°C. The Raman spectrum of TiO_2 nanopowder measured at room temperature after heating at 900°C (1173 K), also shown in Fig. 2(a), confirms the crystallite growth due to heating. Namely, the position (143.5 cm^{-1}) and linewidth (8.8 cm^{-1}) of the E_g Raman mode in this spectrum are close to their values characterstic for the Raman spectrum of polycrystalline anatase TiO_2 [12].

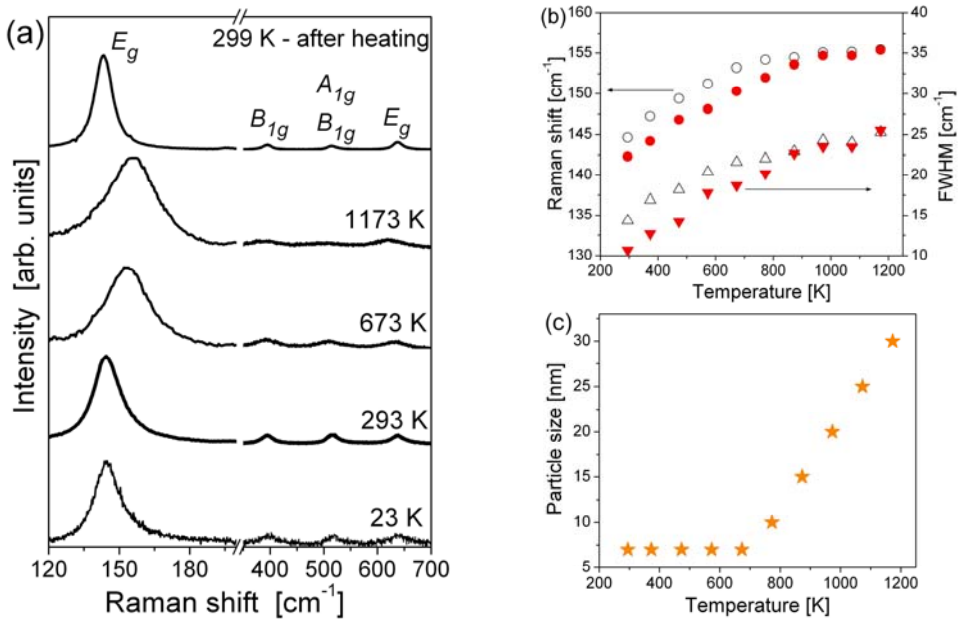

FIGURE 2. Raman spectra of anatase TiO_2 nanopowder taken at different temperatures (a). As-read experimental (open symbols) and calculated (full symbols) positions and halfwidths of Raman E_g mode (b) and the temperature dependence of particle size obtained from fitting procedure (c).

These results have shown that the contributions of confinement effect and nonstoichiometry due to laser irradiation in vacuum are pronounced at low temperatures. However, at high temperatures the contribution due to anharmonic effect is dominant. Decreasing of phonon confinement effect with temperature increase is ascribed to the crystallite growth at temperatures higher then 773 K.

Raman spectra of ZnO powders

Raman spectra of the commercial zinc oxide powder (ZnO(0)) and mechanically activated powders with grinding time of 30 min (ZnO(30)) and 300 min (ZnO(300)) are presented in Fig. 3. The Raman modes of the original sample can be assigned to the Raman spectra of the bulk ZnO [16]. In the spectra of activated ZnO powders the intensity of all observed modes decreases and their linewidth increases, while E_2^{high} and E_1(LO) modes shift to lower wavenumber with increasing activation time. As grain size in the powders is relatively great (44 nm for ZnO(300), 106 nm for ZnO(30) and 190 nm for ZnO(0)), the application of the phonon confinement model gives symmetrical Raman mode shape without shift. Having in mind the microstrain values (from XRD), which drastically increase with activation time (~0.04 % for ZnO(0), ~0.32 % for ZnO(30), and ~0.78 % for ZnO(300)), the broadening and redshift of E_2^{high} and E_1(LO) modes originate from tensile strain effects introduced by mechanical activation, rather then the effects of phonon confinement [16, 22].

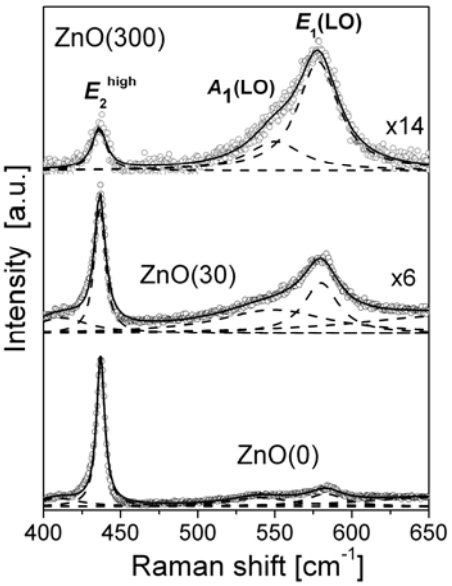

FIGURE 3. Experimental (o) and calculated (thick line) Raman spectra of ZnO powders. Thin lines denote Lorentzian peaks originating from assigned Raman modes.

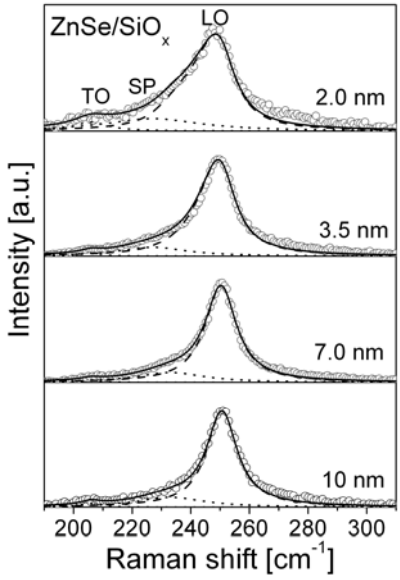

FIGURE 4. Normalized experimental Raman spectra (o) of ZnSe/SiO_x multilayers and calculated results (thick line). Dotted lines denote TO and SP Lorentzian peaks. Dashed line represents LO mode calculated from 1D phonon confinement model.

Raman scattering from ZnSe/SiO_x multilayers

The experimental and calculated Raman spectra of ZnSe/SiO_x multilayers with ZnSe layer thickness of 2.0, 3.5, 7.0 and 10 nm [17] are shown in Fig. 4. The calculated spectra are obtained as sum of contributions of longitudinal (LO) and transversal (TO) optical modes and surface phonon mode (SP). The influence of ZnSe

layer thickness on frequency shift and asymmetrical broadening of the LO Raman mode at ~251 cm^{-1} is analyzed by applying an one-dimensional (1D) phonon confinement model. With the layer thickness decreases, the Raman mode position is blueshifted and asymmetricaly broadened. Applied 1D phonon confinement model gives very good results in estimation of LO mode position and width and allows us to assume that ZnSe in $ZnSe/SiO_x$ multilayers can be treated as nanolayers rather than isolated or loosely connected nanoparticles [17].

INFRARED SPECTROSCOPY

IR spectra of laser synthesized anatase TiO_2 nanopowders

The IR reflection spectra of laser synthesized anatase TiO_2 nanopowder samples with different particle size: 14, 16 and 23 nm are shown in Fig.5(a). The calculations of IR spectra were done using Bruggeman effective medium approximation (EMA), which takes into account the macroscopic volume fractions and local microstructural geometry of the material [20]. The IR spectra of anatase TiO_2 nanopowders are analyzed in three steps, using (i) bulk data, (ii) the polycrystalline character of the nanopowder and (iii) the porosity of the nanopowder, together with the influence of pore shape [20]. In Fig 5. the calculated spectra for the adjustable depolarization factor L=0.65 and TiO_2 volume fractions (f_{TiO2}) from 0.55 to 0.75 are also presented. It is obvious that a decrease in f_{TiO2} causes a broadening of IR features. The physical reason for such behavior lies in the fact that the smaller f_{TiO2} (the greater the porosity) is, the smaller is the particle size.

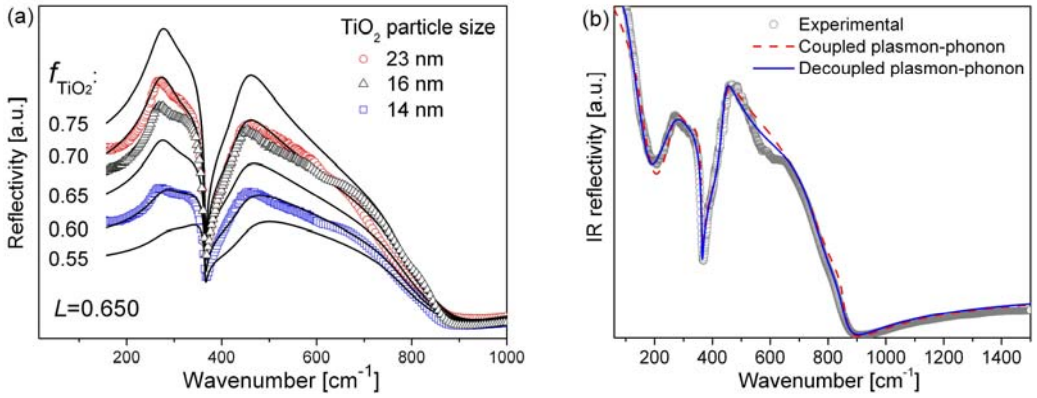

FIGURE 5. (a) Experimental (o) and calculated (—) IR spectra of TiO_2 nanopowders with particle size denoted. (b) Experimental (o) and fitted spectra of nonstoichiometric TiO_2 nanopowder.

The infrared spectrum of nonstoichiometric TiO_2 is presented in Fig. 5(b) by open circles. The appearance of a strong plasmon mode points to the presence of great number of free carriers, introduced by nonstoichiometric defects, mainly oxygen vacancies at the surface of grains. Model for IR spectra based on generalized

Bruggeman EMA, including factorized form of dielectric function is used to analyze the plasmon contribution. Fitted spectra corresponding to coupled LO-phonon-plasmon modes (dashed line), and by using decomposed factorized form of dielectric function, with independent lattice and plasmon parameters (solid line) are presented also in Fig. 5(b). Both spectra are fitted by generalized Bruggeman EMA, with volume fraction f_{TiO2}=0.62 and pore shape factor L=0.65 [21].

Good qualitative and quantitative agreement between theoretical and experimental IR spectra and compatibility of the fitting results with the physical properties of TiO_2 nanopowders as well, confirm the validity of the proposed model.

IR spectra of ZnO powders

Far infrared (IR) reflectivity spectra of ZnO commercial and mechanically activated powders are shown in Fig. 6. The differences between IR spectra of original and activated samples point out to the changes in the powder microstructure. Moreover, a new IR band at ~380 cm^{-1} appears in the spectrum of ZnO(300), besides A_1 and E_1 infrared active modes characteristic for ZnO, indicating the presence of a small amount of iron-oxides due to long time grinding in a vibro-mill with steel rings [22].

This study confirms IR spectroscopy methods as very useful in determination of microstructural properties and detection of unintentionally introduced impurities in the material.

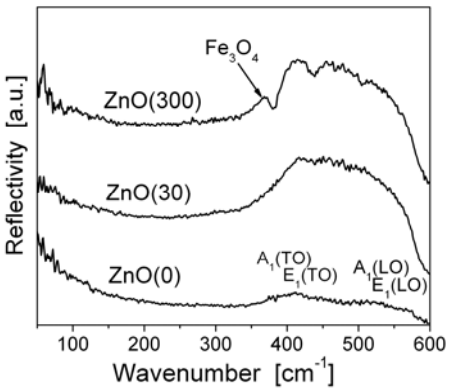

FIGURE 6. IR reflectivity spectra of commercial (ZnO(0)) and mechanically activated ZnO powders for 30 (ZnO(30)) and 300 (ZnO(300)) minutes.

CONCLUSION

We have shown that Raman and infrared spectroscopy are very effective and nondestructive optical techniques for characterization of nanostructure materials.

The experimental Raman spectra presented here, as well as their analyses based on phonon confinement model, confirm Raman spectroscopy as powerful technique for determination the structural properties of nanomaterials. From Raman measurements we can easily estimate average particle size (layer thickness) and its distribution, strain

and anharmonic effects, nonstoichiometry and structural defects. Raman scattering is also very useful in investigation of stability of nanostructured materials at different temperature and under different environmental conditions.

The infrared spectra give possibility to obtain wide range of information on nanostructured material, such as particle size, porosity, structural defects and nonstoichiometry.

ACKNOWLEDGMENTS

This work was supported by the MSRS under the projects No. 141047 and 142040 and the OPSA-026283 Project within EC FP6 Programme.

REFERENCES

1. Gouadec, G., Colomban, P., *Progress in Crystal Growth and Characterization of Materials* **53**, 1-56 (2007).
2. Bassi, A. Li, et al.., *J. Appl. Phys*. **98**, 074305 (2005).
3. Kelly, S., Pollak, F. H., Tomkiewicz, M., *J. Phys. Chem. B* **101**, 2730 (1997).
4. Bersani, D., Lottici, P. P., *Appl. Phys. Lett*. **72**, 73 (1998).
5. Zhang, W. F., He, Y. L., Zhang, M. S., Yin, Z., Chen, Q., *J. Phys. D: Appl. Phys*. **33**, 912 (2000)**.**
6. Šćepanović, M. J., Grujić-Brojčin, M. U., Dohčević-Mitrović, Z. D., Popović, Z. V., *Materials Science Forum* **518**, 101 (2006).
7. Richter, H., Wang, Z.P., Ley, L., *Solid State Commun.* **39**, 625 (1981).
8. Campbell, I. H., Fauchet, P.M., *Solid State Commun.* **58**, 739 (1984).
9. Spanier, J. E., Robinson, R. D., Zhang, F., Chan, S. W., Herman, I. P., *Phys. Rev. B* **64**, 245407 (2001).
10. Santos, D. R., Torriani, I. L., *Solid State Commun.* **85**, 307 (1993).
11. Parker, J. C., Siegel, R. W., *Appl. Phys. Lett.* **57**, 943 (1990).
12. Zhu, K. R., Zhang, M. S., Chen, Q., Yin, Z., *Phys. Lett. A* **340**, 220 (2005).
13. Arora, A. K., Rajalakshmi, M., Ravindran, T. T., in *Encyclopedia of Nanoscience and Nanotechnology*, ed. H. S. Nalwa, American Scientific Publishers, 2004, Vol. X, p.1.
14. Dohčević-Mitrović, Z. D., Šćepanović, M. J., Grujić-Brojčin, M. U., Popović, Z. V., Bošković, S. B., Matović, B. M., Zinkevich, M. V., and Aldinger, F., *Solid State Commun* **137**, 387 (2006).
15. Šćepanović, M. J., Grujić-Brojčin, M., Dohčević-Mitrović, Z. D., Popović, Z. V., *Appl. Phys. A* **86**, 365–371 (2007).
16. Šćepanović, M., Srećković, T., Vojisavljević, K., Ristić, M. M., *Sci. Sintering* **38,** 169 (2006).
17. Šćepanović, M. J., Grujić-Brojčin, M., Bineva, I., Nesheva, D., Aneva, Z., Levi, Z., Popović, Z. V., *J. Optoelectron. Adv. Mat.* **9,** 178–181 (2007).
18. Popović, Z. V, Dohčević-Mitrović, Z. D., Konstantinović, M. J., Šćepanović, M., *J. Raman Spectrosc.* **38**, 750-755 (2007).
19. Šćepanović, M., Grujić-Brojčin, M., Dohčević-Mitrović, Z. D, Popović, Z. V, submitted
20. Grujić-Brojčin, M., Šćepanović, M. J., Dohčević-Mitrović, Z. D., Hinić, I., Matović, B., Stanišić, G., Popović, Z. V., *J. Phys. D: Appl. Phys* **38**, 1415 (2005).
21. Grujić-Brojčin, M., Šćepanović, M., Dohčević-Mitrović, Z., and Popović, Z. V., *Sci. Sintering* **38,** 183-189 (2006)
22. Šćepanović, M. J., Dohčević-Mitrović, Z. D., Srećković, T., Vojisavljević, K., and Popović, Z. V., *Sixth International Conference of the Balkan Physical Union,* edited by S. A. Cetin and I. Hikmet, American Institute of Physics, 2007, p. 648
23. Balaji, S., Djaoued, Y., and Robichaud, J., *J. Raman Spectrosc* **37**, 1416–1422 (2006).